Physica E 45 (2012) 190–193

Contents lists available at SciVerse ScienceDirect

Physica E

journal homepage: www.elsevier.com/locate/physe

Relative stability of nanosized β-C_3N_4 and graphitic C_3N_4 from first principles calculations

Junting Luo [a], Bin Wen [a,*], Roderick Melnik [b,c]

[a] State Key Laboratory of Metastable Materials Science and Technology, Yanshan University, Hebei Street West 438, Qinhuangdao 066004, China
[b] M²NeT Lab, Wilfrid Laurier University, Waterloo, 75 University Avenue West, Ont., Canada N2L 3C5
[c] Ikerbasque, Basque Foundation for Science and BCAM, 48011, Bilbao, Spain

HIGHLIGHTS

- Relative stability of nanosized C_3N_4 has been studied.
- Nanosized β-C_3N_4 becomes more stable than the g-C_3N_4 phase.
- Electronic properties of nanosized C_3N_4 have been analyzed.

ARTICLE INFO

Article history:
Received 4 January 2012
Received in revised form
27 July 2012
Accepted 1 August 2012
Available online 10 August 2012

ABSTRACT

Relative stability of nanosized β-C_3N_4 and graphitic C_3N_4 has been studied by using first principles calculations. It has been demonstrated that the relative stability sequence changes with increasing size of the nanostructure. When the number of C_3N_4 molecules in the C_3N_4 nanostructure is less than a threshold number, the β-C_3N_4 nanostructure is in the stability phase. When the number of C_3N_4 molecules in the C_3N_4 nanostructure exceeds the threshold number, the graphitic C_3N_4 is in the stability phase. In addition, size-dependence electronic properties of β-C_3N_4 and graphitic C_3N_4 nanostructures have also been analyzed in this work.

1. Introduction

Based on the first principles calculations, the bulk modulus and hardness of β-C_3N_4 phase were predicted to be similar to those of diamond by Liu and Cohen in 1989 [1]. Hereafter, many theoretical [2–4] and experimental works [5–16] have been performed to study and synthesize this potentially superhard material. In spite of these effects, there has been no unambiguous evidence of successful synthesis of β-C_3N_4 phase crystallization with stoichiometric C_3N_4 composition to date [5]. In many experiments [11–16], the final product is mainly amorphous carbon nitride compound. However, in some experimental works (e. g. [11]), some nanosized β-C_3N_4 crystals embedded in the amorphous carbon nitride compound matrix have been found. It is worth noting that many nanosized dense phases are more thermodynamically stable than the corresponding nanosized lower dense phases [17–20]. These facts imply that nanosized dense β-C_3N_4 crystals may be in a more thermodynamically stable phase compared to the nanosized lower dense graphitic C_3N_4 (g-C_3N_4) phase. To verify this hypothesis, an accurate description of the relative stability of nanosized β-C_3N_4 and g-C_3N_4 structures has been presented in this work. The heats of formation for a number of β-C_3N_4 and g-C_3N_4 nanostructures have been found by first principle calculations. Our results indicate that the β-C_3N_4 phase for the number of molecules smaller than a threshold numbers becomes thermodynamically more stable than the g-C_3N_4 phase.

2. Computational method

In this contribution, we analyze in detail a series of nanosized β-C_3N_4 prism structures and a series of nanosized g-C_3N_4 sheets with D3h symmetry and various side lengths. For the prism β-C_3N_4 nanostructures, three kinds of nanostructures with different cross sections have been considered here, that is, 2×2, 2×1 and 1×1 cross sections, where the numbers represent parallelogram cross section side lengths. For example, 2×2 means that the two parallelogram cross section side lengths are two times of β-C_3N_4 lattice $\boldsymbol{a}$. For every nanostructure considered here, the outer dangling bonds were fully terminated by hydrogen atoms. Such treatment corresponds to experimental measurements of hydrogen existence in g-C_3N_4 from decomposition of melamine [21]. Hence, the hydrogen terminated C_3N_4 clusters considered

* Corresponding author. Tel.: +86 335 8568761.
E-mail address: wenbin@ysu.edu.cn (B. Wen).

1386-9477/$ - see front matter © 2012 Elsevier B.V. All rights reserved.
http://dx.doi.org/10.1016/j.physe.2012.08.001

here include $C_{24}H_{64}N_{32}$, $C_{48}H_{80}N_{64}$, $C_{72}H_{96}N_{96}$, $C_{96}H_{112}N_{128}$, and $C_{120}H_{128}N_{160}$ for the 2×2 cross section β-C_3N_4 nanostructure, $C_{12}H_{36}N_{16}$, $C_{24}H_{48}N_{32}$, $C_{36}H_{60}N_{48}$, $C_{48}H_{72}N_{64}$, $C_{60}H_{84}N_{80}$, $C_{72}H_{96}N_{96}$, and $C_{84}H_{108}N_{112}$ for the 2×1 cross section β-C_3N_4 nanostructure, $C_6H_{20}N_8$, $C_{12}H_{28}N_{16}$, $C_{18}H_{36}N_{24}$, $C_{24}H_{44}N_{32}$, $C_{30}H_{52}N_{40}$, $C_{36}H_{60}N_{48}$, $C_{42}H_{68}N_{56}$, $C_{48}H_{76}N_{64}$, $C_{54}H_{84}N_{72}$, $C_{60}H_{92}N_{80}$, and $C_{66}H_{100}N_{88}$ for the 1×1 cross section β-C_3N_4 nanostructure, and $C_3H_6N_6$, $C_9H_9N_{15}$, $C_{18}H_{12}N_{28}$, $C_{30}H_{15}N_{45}$, $C_{45}H_{18}N_{66}$, $C_{63}H_{21}N_{91}$, $C_{84}H_{24}N_{120}$, $C_{108}H_{27}N_{153}$, $C_{135}H_{30}N_{190}$, as well as $C_{165}H_{33}N_{231}$ for the g-C_3N_4 nanostructure. Fig. 1 shows two representative structures for a β-C_3N_4 nanostructure of $C_{120}H_{128}N_{160}$ and a g-C_3N_4 nanostructure of $C_{165}H_{33}N_{231}$. Owing to symmetry breaking of g-C3N4 nanostructures, the proportion of N:C in a g-C3N4 nanostructure is larger than 4:3.

The geometries for these nanosized β–C_3N_4 and g-C_3N_4 were optimized using a density functional theory (DFT) with effective core potentials implemented in the DMOL package [22,23]. We used a double numerical basis including a *d*-polarization function (DND) and adopted the generalized gradient approximation (GGA) with the PBE parameterization [24] to describe the exchange-correlation interaction. First, we optimized the lattice parameters of the bulk g-C_3N_4. The lattice parameters ***a*** and ***c***, obtained for bulk g-C_3N_4, are 4.742 and 6.721 Å respectively, which agree well with the experimental and previous theoretically predicted values [3]. This confirmed that the computation scheme used in this paper is reliable.

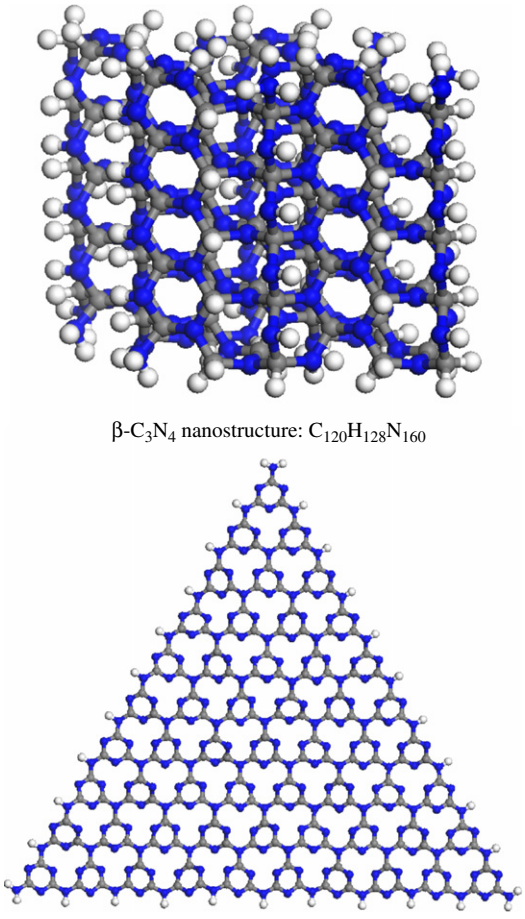

Fig. 1. Atomic structures of the representatives of a β-C_3N_4 nanostructure of $C_{120}H_{128}N_{160}$ and a g-C_3N_4 nanostructure of $C_{165}H_{33}N_{231}$. Gray ball: carbon; white ball: hydrogen; blue ball: nitrogen. (For interpretation of the references to color in this figure legend, the reader is referred to the web version of this article.)

3. Results and discussions

To study the relative stability between hydrogen terminated β-C_3N_4 and g-C_3N_4 nanostructures, the heats of formation per C_3N_4 molecule have been calculated by using the following formula:

$$E_{form}^{(C_3N_4)_mH_nN_s}=\left(E_{total}^{(C_3N_4)_mH_nN_s}-mE_{graphitic}^{C_3N_4}-\frac{n}{2}E_{gas}^{H_2}-\frac{s}{2}E_{gas}^{N_2}\right)/m \quad (1)$$

where $E_{form}^{(C_3N_4)_mH_nN_s}$ is the heat of formation per C_3N_4 molecule for a $C_{3m}H_nN_{4m+s}$ nanostructure, $E_{total}^{(C_3N_4)_mH_nN_s}$ refers to the total energy of a relaxed $C_{3m}H_nN_{4m+s}$ nanostructure that includes $3m$ C atoms, n H atoms and $4m+s$ N atoms, $E_{graphitic}^{C_3N_4}$is the total energy per C_3N_4 molecule in g-C_3N_4 solid, $E_{gas}^{H_2}$ is the total energy of a H_2 molecule and $E_{gas}^{N_2}$ is the total energy of a N_2 molecule. As mentioned, the geometries of these hydrogen terminated C_3N_4 nanostructures were optimized by using the DFT with effective core potentials implemented in the DMOL package, and the total energies for these optimized nanostructures were obtained. The heats of formation for these nanostructures have been calculated by using Eq. (1), and the relationship between the heats of formation and the size for various phases of hydrogen terminated C_3N_4 nanostructures have been plotted in Fig. 2. The heats of formation per C_3N_4 molecule, $E_{form}^{(C_3N_4)_mH_nN_s}$, as a function of the number of C_3N_4 molecules in the nanostructure is shown in Fig. 2a. Note that with the increase in the number of C_3N_4 molecules, the heat of formation per C_3N_4 molecule, $E_{form}^{(C_3N_4)_mH_nN_s}$, for both β-$C_3N_4$ and g-C_3N_4 nanostructures, increases monotonously. Fig. 2b shows the heat of formation per C_3N_4 molecule, $E_{form}^{(C_3N_4)_mH_nN_s}$, as a function of cluster size inverse $m^{-1/3}$, where m is the number of C_3N_4 molecules in these hydrogen terminated C_3N_4 nanostructures. As can be seen from Fig. 2b, the heat of formation per C_3N_4 molecule, $E_{form}^{(C_3N_4)_mH_nN_s}$, decreases with cluster size inverse $m^{-1/3}$for all nanostructures studied in this work. It is known that the ratio of surface atom number and internal atom number increases with increasing of cluster size inverse $m^{-1/3}$, therefore, with increasing of surface atom number, the heat of formation for C_3N_4 nanostructure decrease. For the 2×2 cross section β-C_3N_4 nanostructure, with increasing cluster size inverse $m^{-1/3}$, the heat of formation per C_3N_4 molecule, $E_{form}^{\beta-C_3N_4}$, can be approximated according to an exponential relationship: $E_{form}^{\beta-C_3N_4}=-0.97\exp(3.14m^{-1/3})+1.98$. For the g-$C_3N_4$ nanostructure, with increasing cluster size inverse$m^{-1/3}$, the heat of formation per C_3N_4 molecule,$E_{form}^{Graphitic}$decreases according to an exponential relationship: $E_{form}^{Graphitic}=-3.81\exp(0.68m^{-1/3})+3.53$. The extrapolated values 1.01 and -0.28 eV/C_3N_4 at the bulk limit compare well to the heats of formation (1.41 and 0 eV/C_3N_4) obtained for the solid β-C_3N_4 and g-C_3N_4 crystals, respectively. This result is an additional confirmation that the computational parameters used in this work are reliable. Note, however, that the heat of formation per C_3N_4 molecule, $E_{form}^{(C_3N_4)_mH_nN_s}$, for both β-$C_3N_4$ and g-C_3N_4 nanostructures is lower than that of bulk C_3N_4. These results also indicate that with decreasing size of C_3N_4 nanostructures, their stability increases. From Fig. 2, it can be seen that there are cross points for the heat of formation curves of β-C_3N_4 and g-C_3N_4 nanostructures, which indicates that the relative stability sequence changes with increasing size of nanostructures. It also suggests that the β-C_3N_4 nanostructure is thermodynamically more stable than the g-C_3N_4 nanostructure when the nanostructure size smaller than a threshold number. However, for different cross section β-C_3N_4 nanostructures, this threshold number is different. More precisely, the threshold numbers are 9, 8 and 4 for 2×2, 2×1 and 1×1 cross

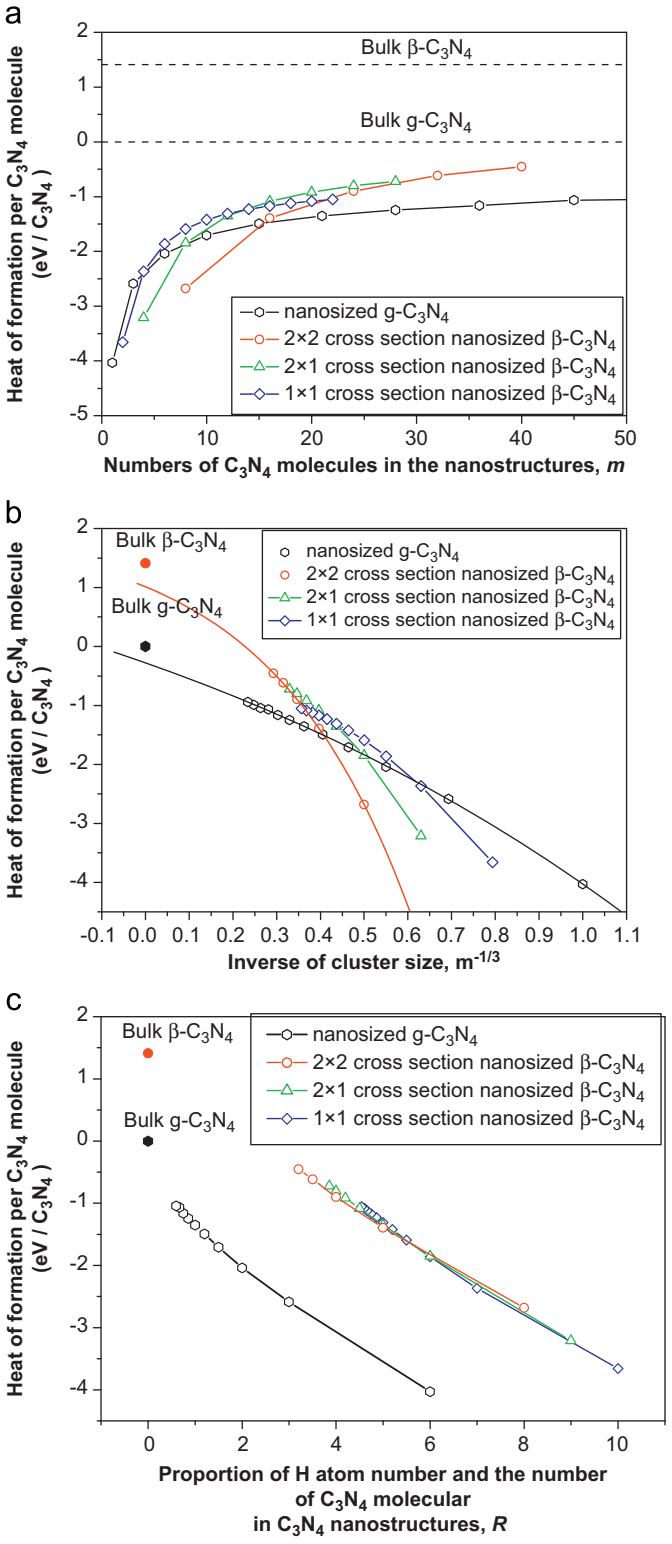

Fig. 2. (a) The total energy per C_3N_4 molecule as a function of the size of C_3N_4 nanostructure. (b) The total energy per C_3N_4 molecule as a function of cluster size inverse $m^{-1/3}$ (m is the number of C_3N_4 molecules in the C_3N_4 nanostructure). (c) Relationships between heat of formation and R (hydrogen concentration) for different C_3N_4 nanostructures.

section β-C_3N_4, respectively. The cross point position (or the threshold number) shift is due to the different hydrogen concentrations and edge atom in different cross section β-C_3N_4 nanostructures. This result implies that the hydrogen concentration and edge atom can affect the relative stability of C_3N_4 nanostructure.

To further study the effect of hydrogen concentration and edge atom on the relative stability and threshold numbers, a proportion of H atoms number n and the number of C_3N_4 molecules m in these hydrogen terminated C_3N_4 nanostructures, $R=\frac{n}{m}$, has been defined, which correspond with the hydrogen concentration in a C_3N_4 nanostructure. In Fig. 2c, a relationship between heat of formation and R for different C_3N_4 nanostructures has been plotted. As can be seen from Fig. 2c, the heat of formation per C_3N_4 molecule decreases with increasing of R for all nanostructures studied in this work, this indicates that the stability increased with increasing hydrogen concentration. For different β-C_3N_4 nanostructures studied in this work, with increasing of R, the heat of formation per C_3N_4 molecule decreases linearly, and the corresponding slopes are approximately same. This result implies that hydrogen concentrations is the main influencing factors on the stability of β-C_3N_4 nanostructures, and edge atom's effect on the stability of β-C_3N_4 nanostructures is less than hydrogen concentrations for these nanostructures studied here. For the g-C_3N_4 nanostructure, the heat of formation per C_3N_4 molecule decreases exponentially with increasing of R. From Fig. 2c, it can be seen that there are no cross points for the heat of formation curves of β-C_3N_4 and g-C_3N_4 nanostructures, this indicates that hydrogen concentrations is different for different type of C_3N_4 nanostructures with same number of C_3N_4 molecules m, and the phase transformation between β-C_3N_4 and g-C_3N_4 nanostructures will have additional hydrogen atoms transformation. It is for this reason that the threshold number is shifted for different type of C_3N_4 nanostructures. Because only three types of β-C_3N_4 nanostructures have been discussed in this work, the edge atom's effect on stability is not obvious. If to further study this effect, many types of β-C_3N_4 nanostructures are needed and this is also our work in future.

To understand the electronic properties of these C_3N_4 nanostructures, size dependent highest occupied molecular orbital/lowest unoccupied molecular orbital (HOMO–LUMO) energy gaps have been calculated and plotted in Fig. 3. Due to a failure of describing systems with localized d and f electrons, the energy gap is often underestimated by using GGA approaches in the DFT scheme [19]. In this work, the experimental band energy gap of g-C_3N_4 is 2.7 eV [25], whereas our calculated band gap is only 1.415 eV. As can be seen from Fig. 3a, for all C_3N_4 nanostructures considered in this work, the calculated HOMO–LUMO energy gap was also estimated from below and it was found that all HOMO–LUMO energy gaps decrease with increasing cluster size. For g-C_3N_4 nanostructures, all HOMO–LUMO energy gaps are larger than that of bulk g-C_3N_4. However, for β-C_3N_4 nanostructures, when the cluster is small, the HOMO–LUMO energy gap is larger than that of bulk β-C_3N_4. At the same time, with increasing cluster size and larger than a threshold number, the HOMO–LUMO energy gap becomes lower than that of bulk β-C_3N_4. The results also indicate that the hydrogen concentration and shape of nanostructures not only affects the relative stability of C_3N_4 nanostructures, but also it affects the electronic properties of β-C_3N_4 nanostructures.

To further study the effect of hydrogen concentration and shape of nanostructures on the electronic properties of C_3N_4 nanostructures, relationships between HOMO–LUMO gap and R for different C_3N_4 nanostructures have been plotted in Fig. 3b, it can be seen that with increasing R, all HOMO–LUMO energy gaps increase. This result also corresponds to the result in Fig. 3a, with decreasing cluster size, the ratio of surface atom number and internal atom number increases and the hydrogen concentration increases. Therefore, the increasing HOMO–LUMO energy gaps not only from size effect but also from surface hydrogen atom effect. Due to the size of nanostructure and surface hydrogen atom concentration is relational in the nanostructure studied in

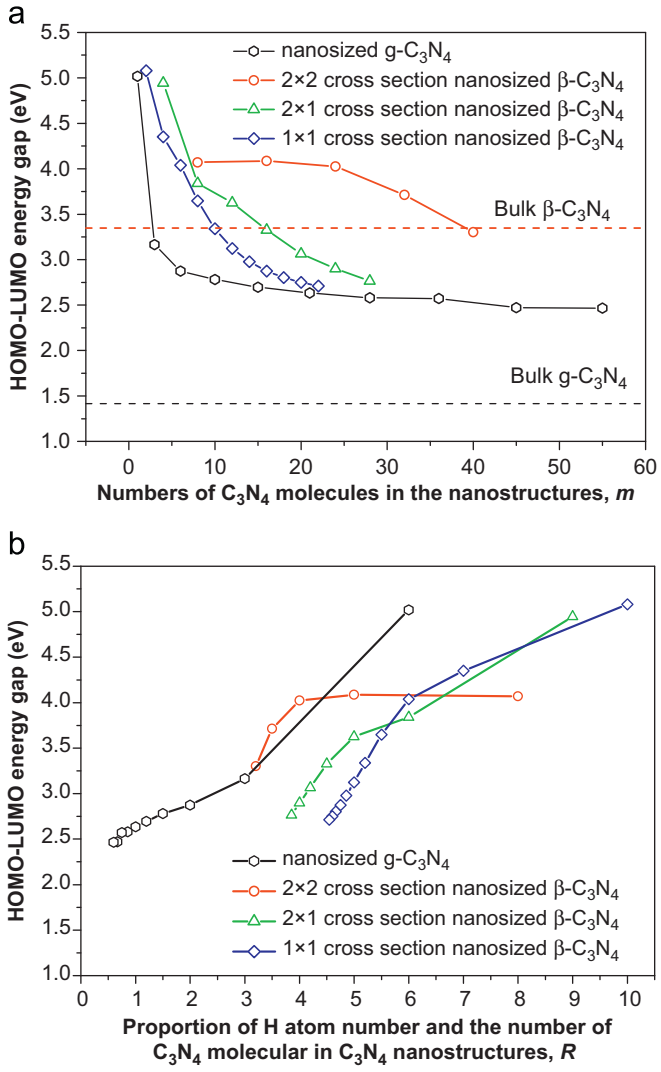

Fig. 3. (a) The HOMO–LUMO gap as a function of the size of C_3N_4 nanostructure. (b) Relationships between HOMO–LUMO gap and *R* (hydrogen concentration) for different C_3N_4 nanostructures.

this work; it is hard to distinguish which factor is a main influencing factor on the HOMO–LUMO energy gaps. Then it is obvious that the shape of nanostructure has a significant effect on the HOMO–LUMO energy gaps, because the fact that the HOMO–LUMO energy gaps is conspicuous different for different shape of C_3N_4 nanostructures with same size or hydrogen concentration (or the value of *R*).

4. Conclusions

In summary, first principle calculations have been carried out to determine the relative stability between g-C_3N_4 and β-C_3N_4 nanostructures. The size dependence HOMO–LUMO energy gaps have also been obtained. Our results indicate that the relative stability sequence changes with increasing size of nanostructures, the β-C_3N_4 nanostructure is thermodynamically more stable than the g-C_3N_4 nanostructure when the nanostructure size is smaller than a threshold number. However, for different cross section β-C_3N_4 nanostructures, this threshold number is different. Finally, it also indicates that the hydrogen concentration not only affects the relative stability of C_3N_4 nanostructure, but it also affects the electronic properties of β-C_3N_4 nanostructures.

Acknowledgments

This work was supported by the National Natural Science Foundation of China (Grant nos. 51121061, and 51131002) and the Key Basic Research Program of Hebei Province of China (No. 12965135D). R.M. acknowledges the support from the NSERC and CRC programs, Canada. This work was made possible by the facilities of the Shared Hierarchical Academic Research Computing Network (SHARCNET:www.sharcnet.ca) and Compute/Calcul Canada.

References

[1] A.Y. Liu, M.L. Cohen, Science 245 (1989) 841.
[2] D.M. Teter, R.J. Hemley, Science 271 (1996) 53.
[3] G. Goglio, D. Foy, G. Demazeau, Materials Science and Engineering R 58 (2008) 195, and the references therein.
[4] C.M. Sung, M. Sung, Materials Chemistry Physics 43 (1996) 1.
[5] L. Fang, H. Ohfuji, T. Shinmei, T. Irifune, Diamond and Related Materials 20 (2011) 819.
[6] L.C. Ming, P.V. Zinin, Y. Meng, X.R. Liu, S.M. Hong, Y. Xie, Journal of Applied Physics 99 (2006) 033520.
[7] P.V. Zinin, L.C. Ming, S.K. Sharma, S.M. Hong, Y. Xie, T. Irifune, T. Shinmei, Journal of Physics: Conference Series 121 (2008) 062002.
[8] V.L. Solozhenko, E.G. Solozhenko, P.V. Zinin, L.C. Ming, J.H. Chen, J.B. Parise, Journal of Physics Chemistry of Solids 64 (2003) 1265.
[9] E. Kroke, M. Schwarz, Coordination Chemistry Reviews 248 (2004) 493.
[10] E. Horvath-Bordon, R. Riedel, A. Zerr, P.F. McMillan, G. Auffermann, Y. Prots, W. Bronger, R. Kniep, P. Kroll, Chemical Society Reviews 35 (2006) 987.
[11] L. Yin, M. Li, Y. Liu, J. Sui, J. Wang, Journal of Physics: Condensed Matter 15 (2003) 309.
[12] J. Liu, T. Sekine, T. Kobayashi, Solid State Communications 137 (2006) 21.
[13] J. Martin-Gil, F.J. Martin-Gil, M. Sarikaya, M. Qian, M. JoseYacaman, A. Rubio, Journal of Applied Physics 81 (1997) 2555.
[14] D.C. Nesting, J.V. Badding, Chemistry of Materials 8 (1996) 1535.
[15] A. Andreyev, M. Akaishi, D. Gobleg, Diamond and Related Materials 11–12 (2002) 1885.
[16] J.L. Zimmerman, R. Williams, V.N. Khabashesku, J.L. Margrave, Nano Letters 1 (2001) 731.
[17] B. Wen, J. Zhao, T. Li, Chemical Physics Letters 441 (2007) 318.
[18] A.S. Barnard, Reports on Progress in Physics 73 (2010) 086502.
[19] B. Wen, R.V.N. Melnik, Applied Physics Letters 92 (2008) 261811.
[20] B. Wen, R. Melnik, Chemical Physics Letters 466 (2008) 84.
[21] A. Thomas, A. Fischer, F. Goettmann, M. Antonietti, J.O. Muller, R. Dchlogl, J. Carlsson, Journal of Materials Chemistry 18 (2008) 4893.
[22] B. Delley, Journal of Chemical Physics 92 (1990) 508.
[23] B. Delley, Journal of Chemical Physics 113 (2000) 7756.
[24] J.P. Perdew, K. Burke, M. Ernzerhof, Physical Review Letters 77 (1996) 3865.
[25] X. Wang, K. Maeda, A. Thomas, K. Takanabe, G. Xin, J.M. Carlsson, K. Domen, M. Antonietti, Nature Materials 8 (2009) 76.